Articles

Thermodynamic Properties of Propane. I. $p-\rho-T$ Behavior from (265 to 500) K with Pressures to 36 MPa†

Mark O. McLinden*

Thermophysical Properties Division, National Institute of Standards and Technology, 325 Broadway, Mailstop 838.07, Boulder, Colorado 80305 USA

The $p-\rho-T$ behavior of high-purity (99.999 %) propane was measured from (265 to 500) K with pressures to 36 MPa with a two-sinker densimeter. The measurements extend from low-density vapor to compressed-liquid states, and the extended critical region was studied extensively. Vapor pressures from (270 to 369) K were also measured. The expanded ($k = 2$) uncertainty in density is ($56 \cdot 10^{-6} \cdot \rho + 0.0013$ kg·m^{-3}) at near-ambient conditions, increasing to ($170 \cdot 10^{-6} \cdot \rho + 0.0013$ kg·m^{-3}) at 500 K and 36 MPa. The uncertainties in temperature and pressure are 0.004 K and ($51 \cdot 10^{-6} \cdot p + 2.0$ kPa), respectively. The analysis for density accounts for the force transmission error in the magnetic suspension coupling of the densimeter and includes corrections for vertical density gradients in the measuring cell. These data, together with other new data and carefully selected literature data, have been used to develop an equation of state covering the entire fluid region from the triple-point temperature to 650 K with pressures to 1000 MPa. New measurements of the isochoric heat capacity and speed of sound and the equation of state are described in companion papers.

1. Introduction

Propane is an important commodity chemical, with primary uses as a fuel and as a chemical feedstock. Propane is also very well suited to be a reference fluid for thermodynamic modeling. It is a nonpolar hydrocarbon that is chemically similar to a broad range of simple hydrocarbons. Its triple-point temperature of 85.525 K and critical temperature of 369.89 K give it one of the longest vapor−liquid saturation lines, in terms of reduced temperature, of any fluid ($T_{tp}/T_{crit} = 0.231$). Practical considerations facilitate experimental measurements of its properties: it is a stable material of low toxicity (although it is, of course, highly flammable). Its critical point is easily accessible, and propane is commercially available in very high purity. As a result of these factors, the thermophysical properties of propane have been extensively studied.

The National Institute of Standards and Technology (NIST), in cooperation with Ruhr-Universität Bochum, Germany, and Helmut-Schmidt-Universität, Hamburg, Germany, has undertaken a project to develop a new equation of state (EOS) for the thermodynamic properties of propane. This is part of a larger, long-term program to develop high-accuracy EOS for a number of important reference fluids, including ethane[1] and the butanes.[2] In recent years, the state of the art of EOS development has progressed considerably; as a result, experimental measurements of ever-lower uncertainties can be effectively utilized. Thus, there is a need for new experimental data on propane.

In the present project, NIST has measured the isochoric (C_V) heat capacity, vapor pressure, and $p-\rho-T$ properties of propane; Glos et al.[3] and Claus et al.[4] at Ruhr-Universität Bochum measured the $p-\rho-T$ properties and vapor pressure; and Meier et al.[5] at Helmut-Schmidt-Universität measured the speed of sound in the liquid phase. These data, together with carefully selected literature data, have been used to develop an equation of state covering the entire fluid region from the triple-point temperature to 650 K with pressures to 1000 MPa. The present paper describes high-accuracy measurements of the $p-\rho-T$ behavior of high-purity (99.999 %) propane from (265 to 500) K with pressures to 36 MPa with a two-sinker densimeter; these included extensive measurements in the vicinity of the critical point. Vapor pressures from (270 to 369) K were also measured. The C_V measurements and equation of state are described in companion papers.[6,7] Detailed comparisons of these new data with the new EOS and also all prior literature data are given by Lemmon et al.[7]

2. Experimental Section

The present measurements utilized a two-sinker densimeter. This type of instrument applies the Archimedes (buoyancy) principle to provide an absolute determination of the density, i.e., a measurement that is independent of calibration fluids. The accuracy of the Archimedes technique has been improved by the use of two sinkers. In particular, the two-sinker technique developed by Kleinrahm and Wagner[8] has proven very successful. This general type of instrument is described by Wagner and Kleinrahm.[9]

2.1. Apparatus Description. The two-sinker densimeter used in this work is described in detail by McLinden and Lösch-Will[10] and Lösch-Will.[11] The instrument is depicted in Figure 1, and a brief description is given here. Two sinkers of nearly the same mass, surface area, and surface material, but made of materials with different densities such that they have very different volumes, are weighed separately with a high-precision balance while immersed in a fluid of unknown density. The fluid density ρ is given by

† Contribution of the National Institute of Standards and Technology. Not subject to copyright in the United States.

* Corresponding author. E-mail: markm@boulder.nist.gov. Tel.: +1-303-497-3580. Fax: +1-303-497-5224.

10.1021/je900124n This article not subject to U.S. Copyright. Published 2009 by the American Chemical Society
Published on Web 11/23/2009

$$\rho = \frac{(m_1 - m_2) - (W_1 - W_2)}{(V_1 - V_2)} \quad (1)$$

where m and V are the sinker mass and volume; W is the balance reading; and the subscripts refer to the two sinkers. The main advantage of the two-sinker method is that adsorption onto the surfaces of the sinkers, systematic errors in the weighing, and other effects that reduce the accuracy of most buoyancy techniques largely cancel.

A magnetic suspension coupling transmits the gravity and buoyancy forces on the sinkers to the balance, thus isolating the fluid sample (which may be at high pressure and/or temperature) from the balance. The central elements of the coupling are two magnets, one on each side of a nonmagnetic, pressure-separating wall. The top magnet, which is an electromagnet with a ferrite core, is hung from the balance. The bottom (permanent) magnet is immersed in the fluid sample; it is held in stable suspension with respect to the top magnet by means of a feedback control circuit making fine adjustments in the electromagnet current. The permanent magnet is linked with a "lifting fork" to pick up a sinker for weighing. A mass comparator balance with a resolution of 1 μg and a capacity of 111 g is used for the weighings. The tantalum sinker has a mass of 60.177 91 g and volume of 3.610 25 cm^3 at 293 K. The titanium sinker has a mass of 60.163 34 g and volume of 13.347 55 cm^3 at 293 K. Both sinkers are gold plated.

Equation 1 must be corrected for magnetic effects; this is described by McLinden et al.[12] In addition to the sinkers, two calibration masses are also weighed. The weighings yield a set of four equations that are solved to yield a balance calibration factor α and a parameter β related to the balance tare (i.e., the magnets and other elements of the system that are always weighed)

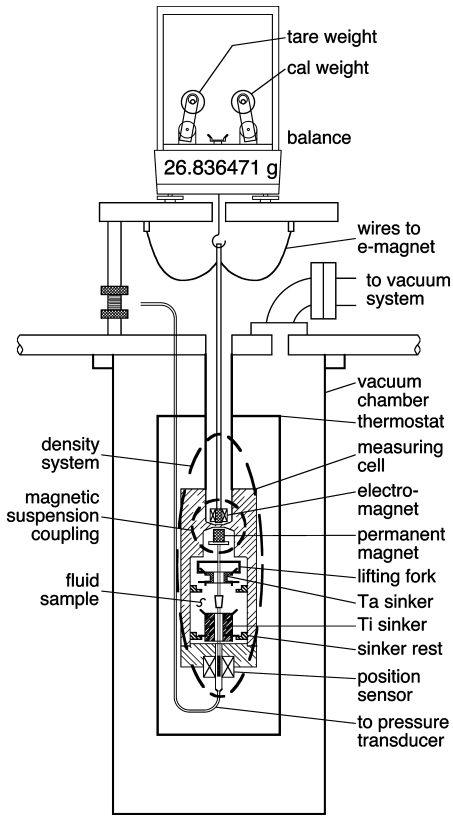

Figure 1. Schematic of the two-sinker densimeter. In this view, the Ta sinker is being weighed, and the Ti sinker is on its rest. Figure is not to scale.

$$\alpha = \frac{W_{cal} - W_{tare}}{(m_{cal} - m_{tare}) - \rho_{air}(V_{cal} - V_{tare})} \quad (2)$$

and

$$\beta = \frac{W_{cal}}{\alpha} - (m_{cal} - \rho_{air}V_{cal}) \quad (3)$$

where the subscripts cal and tare refer to the calibration weights and ρ_{air} is the density of the air (or purge gas) surrounding the balance and is calculated from the ambient temperature, pressure, and humidity measured in the balance chamber. The fluid density ρ_{fluid} is given by

$$\rho_{fluid} = \left[(m_1 - m_2) - \frac{(W_1 - W_2)}{\alpha\phi}\right] \Big/ (V_1 - V_2) - \rho_0 \quad (4)$$

where ρ_0 is the indicated density when measured in a vacuum. In other words, ρ_0 is an "apparatus zero," which compensates for any changes in alignment or sinker masses. The "coupling factor" ϕ, which is the efficiency of the force transmission of the magnetic suspension coupling, is given by

$$\phi = \frac{(W_1/\alpha) - \beta}{m_1 - \rho_{fluid}V_1} \quad (5)$$

Combining the above equations yields the fluid density in terms of directly measured quantities

$$\rho_{fluid} = \left[(m_1 - m_2) - \frac{(W_1 - W_2)m_1}{W_1 - \alpha\beta}\right] \Big/ \left[(V_1 - V_2) - \frac{(W_1 - W_2)V_1}{W_1 - \alpha\beta}\right] - \rho_0 \quad (6)$$

The key point of the analysis by McLinden et al.[12] is that the density given by eq 6 compensates for the magnetic effects of both the apparatus and the fluid being measured. For this apparatus, the coupling factor is nearly unity, and for the present results it varied from 1.000 015 for vacuum to 0.999 978 for propane at the highest density measured (except near the critical point as discussed in Section 4.3).

In addition to the measuring cell, sinkers, suspension coupling, and balance that make up the density measuring system, the apparatus includes a thermostat, pressure instrumentation, and a sample handling system.

The temperature is measured with a 25 Ω standard platinum resistance thermometer (SPRT) and resistance bridge referenced to a thermostatted standard resistor. The signal from the SPRT is used directly in a digital control circuit to maintain the cell temperature constant within ± 0.001 K. The pressures are measured with vibrating-quartz-crystal type pressure transducers. One of three transducers, with maximum pressures of 1.38 MPa, 6.89 MPa, and 41.4 MPa, was used, depending on the pressure range. The transducers (as well as the pressure manifold) are thermostatted to minimize the effects of variations in laboratory temperature.

The thermostat isolates the measuring cell from ambient conditions. It is a vacuum-insulated, cryostat-type design. The measuring cell is surrounded by an isothermal shield, which thermally isolates it from variations in ambient temperature; this shield was maintained at a constant (± 0.01 K) temperature 1 K below the cell temperature by means of electric heating. Additional electric heaters on the cell compensate for the small heat flow from the cell to the shield and allow millikelvin-level control of the cell temperature. Operation at subambient

temperatures was effected by circulating an ethylene glycol solution from a chiller through channels in the shield.

2.2. Experimental Procedures. Measurements were carried out along both isotherms and pseudoisochores (that is, varying temperature, but nearly constant density). Most of the vapor-phase and near-critical measurements and about one-half of the liquid-phase measurements were made along pseudoisochores. The measuring cell was filled at a relatively high density and low temperature. After several replicate points were measured at the desired temperature, the cell was heated to the next, higher set-point temperature, and measurements were made at that temperature. When measurements at the maximum temperature were completed, the cell was cooled, and a portion of the propane charge was vented into a waste bottle. Measurement of the next isochore then commenced. (In adjusting the sample charge, care was taken to remain in the single-phase region. This is not essential for a pure fluid, but excursion into the two-phase region could lead to composition shifts if a mixture was being measured.)

For measurements along isotherms, the measuring cell was pressurized with a manually operated piston-type pressure generator. After completing measurements at a given pressure, the pressure was decreased by extracting a portion of the charge into the pressure generator.

The measurements comprised four separate fillings of propane. The cell was evacuated between fillings (and also prior to the first filling and after the final filling), and measurements were carried out in a vacuum to determine the ρ_0. A fresh sample was used for each filling.

Vapor pressures were measured in conjunction with the $p-\rho-T$ measurements. At the conclusion of fillings 1, 3, and 4, a portion of the sample was vented so that the measuring cell was partially filled with liquid. The densimeter was then used as a static vapor pressure instrument (densities were not measured).

2.3. Experimental Material. The supplier's specification for the propane was a purity of 99.999 %. Our own analysis by gas chromatography combined with mass spectrometry and infrared spectrophotometry (carried out according to the protocols of Bruno and Svoronos[13,14]) revealed only very small impurity peaks that were too small to permit identification. The sample was degassed by freezing in liquid nitrogen and evacuating the vapor space. The sample bottle was connected to a vacuum system at 0.003 Pa; on opening the valve to the frozen sample, the pressure did not increase, indicating that the sample contained virtually no dissolved air. A total of three freeze−pump−thaw cycles were carried out. The sample used in the densimeter was collected and analyzed again following the measurements, and no change in the purity was detected.

3. Uncertainty Determination

We claim a very high accuracy for this instrument, and such claims need to be justified. This instrument provides an absolue determination of the density, so it is not sufficient to merely calibrate it against a well-known reference fluid. In fact, this instrument has been used to certify NIST Standard Reference Materials for density,[15] and this imposes the requirement of a rigorous determination of uncertainties and traceability to fundamental SI quantities. McLinden and Splett[15] provide a detailed analysis of uncertainties for liquid-phase measurements, and McLinden and Lösch-Will[10] provide an analysis of gas-phase uncertainties. Those results are summarized here.

Uncertainty in the density calculated with eq 6 arises from uncertainties in the sinker volumes (V_1, V_2), weighings of the sinkers and calibration masses (W_1, W_2, W_{cal}, W_{tare}), knowledge of the sinker masses (m_1, m_2) and calibration masses (m_{cal}, m_{tare}), and the apparatus zero (ρ_0). Uncertainties in the volumes of the calibration masses (V_{cal}, V_{tare}) and the density of air in the balance chamber (ρ_{air}) have an insignificant contribution because $V_{cal} \approx V_{tare}$.[15] McLinden and Splett[15] have shown that uncertainties in V_1 and V_2 dominate the overall uncertainty in density. The sinker volumes were determined at 293.15 K by use of a hydrostatic comparator. This technique is described by Bowman et al.,[16,17] and our implementation of it is described in ref 15. The sinker volumes at 20 °C were adjusted for temperature with linear thermal expansion data for tantalum and titanium measured over the range (100 to 778) K using samples taken from the same stock of Ta and Ti used to fabricate our sinkers.[10] The sinker volumes were further adjusted by use of an analysis of low-density gas data, as detailed by McLinden.[18] The sinker volumes were adjusted for pressure effects using literature values for the bulk modulus. This correction contributes an uncertainty of $46 \cdot 10^{-6} \cdot \rho$ to the density at 36 MPa. The combined standard uncertainty in the sinker volume difference ($V_1 - V_2$) is estimated to be $28 \cdot 10^{-6} \cdot (V_1 - V_2)$ at 293 K and atmospheric pressure increasing to $85 \cdot 10^{-6} \cdot (V_1 - V_2)$ at 500 K and 36 MPa.

At low densities, errors in the weighings have a significant effect on the uncertainty in density. The standard deviations observed in replicate weighings ranged from 0.2 μg to 5.2 μg for the different objects, and these contribute an uncertainty in density of 0.0005 kg·m^{-3}. The uncertainty in the object masses ranged from 21 μg to 50 μg. Because of the differential nature of the two-sinker method, these contribute only $2 \cdot 10^{-6}$ to the relative uncertainty in density. An automated calibration of the mass comparator is an integral part of each density determination; it is achieved by a mechanism that lowers tare and calibration masses onto a modified balance pan. The masses are cylindrical in shape and fabricated of titanium (tare mass) and stainless steel (calibration mass) with a mass difference of 24.5 g. The different densities of the titanium and stainless steel allow the masses to be nearly identical in volume and surface area. This provides a balance calibration (eq 2) that is (nearly) independent of air buoyancy.

The ρ_0 was determined by repeated measurements of vacuum between each of the fillings. These points were then fitted with straight lines that were interpolated in time to yield the ρ_0 for any given density determination. The ρ_0 changed by 0.0011 kg·m^{-3} to 0.0024 kg·m^{-3} between fillings. This effect contributes a standard uncertainty of 0.000 42 kg·m^{-3} to the density.

The magnetic suspension coupling (MSC) transmits the buoyancy force on the sinkers to the balance, and any systematic error resulting from the influence of nearby magnetic materials could seriously affect the density measurement. This is known as a "force transmission error" (FTE).[9] The analysis of McLinden et al.[12] demonstrated that such errors can be accounted for, reducing the standard uncertainty from this effect to $2 \cdot 10^{-6} \cdot \rho$. On the basis of the vacuum weighings carried out over the course of the present study, the average force transmission error was 915 μg, with a standard deviation $\sigma = 78$ μg. This is equivalent to 0.001 52 % of the 60 g sinker mass. (Strictly speaking, of course, the *force* transmission error should be expressed in units of newtons, but it was measured with a balance that effectively multiplied forces by the acceleration of gravity, giving results in mass units.) The relative effect of temperature over the range (250 to 500) K on the FTE was less than $2 \cdot 10^{-6}$. The relative effect of air versus nitrogen under the balance hood was less than $2 \cdot 10^{-6}$.

Additional factors potentially impacting the density uncertainty are the purity and stability of the test sample. As stated above, the sample was very pure (99.999 %), and we found no evidence of decomposition when analyzing sample removed after the measurements. The impurities accounting for the final 0.001 % of the sample were most likely air (N_2 and O_2), water, and/or other light hydrocarbons, such as ethane; all these have molecular masses lower than that of propane. A 0.001 % impurity with a molar mass of 26 g·mol^{-1} (average of the likely impurities) would affect the molar densities at a relative level of $4 \cdot 10^{-6}$, assuming ideal mixing.

The overall expanded ($k = 2$) uncertainty in the density is

$$U(\rho)/\mathrm{kg{\cdot}m^{-3}} = 2[\{28\}^2 + \{0.37|(T/\mathrm{K} - 293)|\}^2 + \{0.64p/\mathrm{MPa}\}^2]^{0.5} \cdot 10^{-6}\rho/\mathrm{kg{\cdot}m^{-3}} + 0.0013 \quad (7)$$

where the term in brackets is from the sinker volume uncertainty, and the final, constant term includes all other uncertanties. The SPRT used to measure the temperature of the fluid was calibrated from (83 to 505) K by use of fixed point cells (argon triple point, mercury triple point, water triple point, indium freezing point, and tin freezing point). This was done as a system calibration, meaning that the PRT was removed from its thermowell in the measuring cell and inserted into the fixed point cell while using the same lead wires, standard resistor, and resistance bridge as was used in the measurements. The standard uncertainty in the temperature, including the uncertainty in the fixed point cells, drift in the PRT and standard resistor, and any temperature gradients, is 2 mK.

The uncertainty in the pressure arises from three sources: the calibration of the transducers, the repeatability and drift of the transducers, and the uncertainty in the hydrostatic head correction. The pressure transducers were calibrated with piston gages. A gas-operated system was used for pressures up to 7 MPa, and a hybrid gas−oil system was used for pressures up to 40 MPa. This calibration was also done in situ by connecting the piston gage to the sample port of the filling and pressure manifold. On the basis of the uncertainties for the piston gages and the repeatability and zero drift observed for these transducers, we estimate the standard ($k = 1$) uncertainty in pressure arising from calibration and transducer repeatability and drift to be ($9 \cdot 10^{-6} \cdot p + 0.03$ kPa) for the low-range transducer ($p <$ 1.38 MPa), ($11 \cdot 10^{-6} \cdot p + 0.17$ kPa) for the midrange transducer ($p < 6.89$ MPa), and ($26 \cdot 10^{-6} \cdot p + 1.0$ kPa) for the high-range transducer. The complete data tables in the Supporting Information of this paper indicate which transducer was used for a given measurement.

For single-phase states well away from saturation, the pressure uncertainty arising from the hydrostatic head correction is estimated to be less than $10 \cdot 10^{-6} \cdot p$. Near saturation, however, this uncertainty increases. The temperature of the filling line that connected the measuring cell with the pressure transducer was known to only ± 2 K, and thus, the state (liquid or vapor) of the fluid within it has higher uncertainties for the vapor-pressure measurements and other near-saturation conditions. The filling line exited the bottom of the measuring cell, and for the vapor pressure measurements, it was filled with liquid for the first part of its length. For measurements at high temperatures, the temperature of the filling line generally decreased from the measuring cell to the pressure transducer; in these cases, the vapor pressure was sufficient to keep the filling line in a compressed liquid state, so that uncertainties in the temperature resulted in only small uncertainties in the fluid density (and thus head correction) within the line. At lower temperatures, however, the temperature of the filling line first dropped as it exited the cell and passed through the "isothermal shield" of the thermostat (which was maintained 1 K below the cell temperature); it then increased as it exited the main thermostat and entered the separate thermostat for the pressure transducers, which was maintained at 313 K. At some point, the fluid flashed from liquid to vapor. A larger scatter is seen in the data near this transition temperature, and an additional term equal to 0.1 times the total hydrostatic head correction has been added to the pressure uncertainty to account for these effects.

For the single-phase vapor $p-\rho-T$ measurements, a similar effect occurs at pressures between (1.30 and 3.5) MPa. A pressure of 1.30 MPa corresponds to the vapor pressure at 311 K, which is just below the temperature of the pressure transducer, and 3.5 MPa is somewhat lower than the critical pressure of 4.25 MPa. At pressures less than 1.30 MPa, the propane in the filling line is always in the vapor phase. Pressures greater than the critical pressure with reduced densities (ρ/ρ_{crit}) less than 0.6 can be obtained only for temperatures greater than the critical temperature. This means that the filling line contained only vapor, and the propane condensed to a liquid only outside the thermostat, where the filling line was horizontal. At intermediate pressures, however, the vapor-to-liquid phase transition could have occurred in the short vertical portion of the filling line passing between the main thermostat (maintained 1 K below the cell temperature) and the pressure transducer thermostat, which was maintained at 313 K. An additional pressure uncertainty of 1.37 kPa (corresponding to the hydrostatic head of that portion of the filling line filled halfway with liquid) was added to the vapor-phase points with $1.30 < p/\mathrm{MPa} < 4.25$ to account for this uncertainty.

The above uncertainties for temperature, pressure, and density are for these quantities in isolation. For purposes of fitting an equation of state, it is customary to assume that the temperature and pressure (or sometimes temperature and density) are known exactly and lump all uncertainties into a single value for the density (or pressure). This overall combined, or state-point, uncertainty is given by

$$u_C(\rho) = \left\{[u(\rho)]^2 + \left[\left(\frac{\partial\rho}{\partial p}\right)_T u(p)\right]^2 + \left[\left(\frac{\partial\rho}{\partial T}\right)_p u(T)\right]^2\right\}^{0.5} \quad (8)$$

where u_C designates a combined uncertainty; u are the individual uncertainties; and the derivatives are evaluated from an equation of state. For near-critical states where deviations in pressure are an appropriate measure of quality (as discussed in Section 4.3), the state-point uncertainty is

$$u_C(p) = \left\{[u(p)]^2 + \left[\left(\frac{\partial p}{\partial\rho}\right)_T u(\rho)\right]^2 + \left[\left(\frac{\partial p}{\partial T}\right)_\rho u(T)\right]^2\right\}^{0.5} \quad (9)$$

For vapor pressure, the corresponding uncertainty is

$$u_C(p_{sat}) = \left\{[u(p)]^2 + \left[\left(\frac{\partial p_{sat}}{\partial T}\right)u(T)\right]^2\right\} \quad (10)$$

These state-point uncertainties are tablulated for each measured point in the Supporting Information.

4. Results and Comparison to Equation of State

4.1. Vapor Pressures. The densimeter was used to measure the vapor pressure of propane from (270 to 369) K. The experimental data are given in Table 1, and deviations with the EOS of Lemmon et al.[7] are shown in Figure 2 together with a comparison with the data of Glos et al.[3] (Table 1 gives only

Table 1. Experimental Vapor Pressure p_{sat} for Propane from T = (270 to 369) K and Relative Deviations of the Experimental Data from Values Calculated with the Equation of State $p_{sat,EOS}$ of Lemmon et al.[7a]

	T / K	p_{sat} / MPa	$100[(p_{sat} - p_{sat,EOS})/p_{sat,EOS}]$
first filling			
	310.000	1.27199	−0.0363
	312.002	1.33337	−0.0076
	314.001	1.39613	−0.0283
	316.000	1.46172	0.0005
	320.002	1.59846	−0.0285
	324.999	1.78274	−0.0261
	330.000	1.98233	−0.0259
	335.001	2.19802	−0.0214
	340.001	2.43071	−0.0160
	345.000	2.68172	0.0032
	350.001	2.95157	0.0025
	355.001	3.24182	−0.0011
	359.999	3.55441	−0.0012
	361.999	3.68637	0.0008
	363.999	3.82244	0.0012
	365.999	3.96297	0.0024
	368.001	4.10852	0.0029
	369.000	4.18288	−0.0054
third filling			
	309.999	1.27232	−0.0078
	319.998	1.59870	−0.0055
	340.000	2.43105	0.0001
	360.000	3.55507	0.0155
fourth filling			
	269.999	0.43074	0.0739
	279.999	0.58191	0.0423
	289.999	0.76928	0.0221
	300.000	0.99745	−0.0240
	309.999	1.27182	−0.0453
	314.999	1.42828	−0.0363
	319.997	1.59843	−0.0191
	324.999	1.78265	−0.0327
	329.999	1.98216	−0.0316
	334.997	2.19775	−0.0269
	339.998	2.43039	−0.0228
	344.998	2.68150	−0.0028
	349.999	2.95132	−0.0015
	354.999	3.24166	−0.0038
	360.000	3.55450	−0.0015
	364.998	3.89197	0.0004

[a] Only one point per temperature T is given; see Supporting Information for all data.

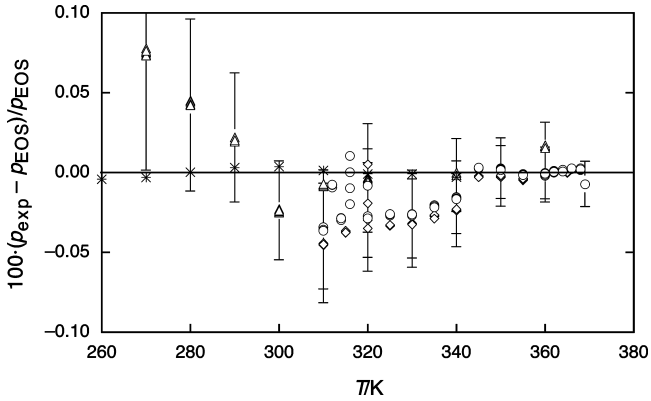

Figure 2. Relative deviations of the experimental vapor pressures p_{exp} for propane from values calculated with the equation of state p_{EOS} of Lemmon et al.[7] ○, This work (filling 1); Δ, this work (filling 2); ◇, this work (filling 4); *, Glos et al.[3] The error bars represent the expanded ($k = 2$) uncertainties for the present data.

one data point for each temperature measured; all of the data are tabulated in the Supporting Information. The companion paper[7] provides a comparison of all the available literature data.)

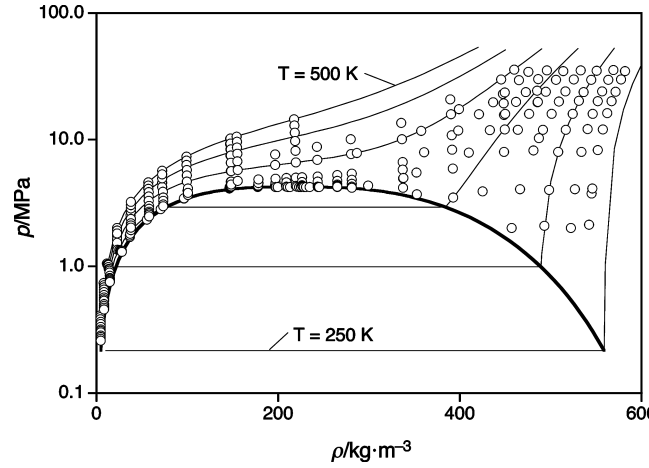

Figure 3. $p-\rho-T$ state points measured for propane in the present work. The bold solid line indicates the saturation boundary, and the fine solid lines indicate isotherms.

The data of Glos et al.[3] were one of the primary data sets used in the EOS fitting, and these data are represented with a relative standard deviation of $28 \cdot 10^{-6} \cdot p$ between (260 and 340) K. The present results were the primary data used at temperatures of 350 K and above, and these are reproduced with a relative standard deviation of $57 \cdot 10^{-6} \cdot p$.

There are small (order of 0.05 %) but significant deviations between the present data and those of Glos et al.[3] At 340 K, there is a discontinuity of about 0.03 % for two of the three fillings. There is also a change in slope at 300 K. These effects are likely related to the hydrostatic head correction as discussed above, which ranges here from (1.36 to 1.86) kPa or from 0.033 % to 0.35 % of the vapor pressure, with the larger relative corrections occurring at the lower temperatures. The error bars indicated in Figure 2 show that the present data agree with the EOS and the data of Glos et al.[3] within their mutual uncertainties, although a number of the points are near the expanded ($k = 2$) uncertainty limit.

4.2. $p-\rho-T$ Data in the Liquid and Vapor Phases. Propane was measured at 296 (T, p) state points from (265 to 500) K with pressures to 36 MPa. Four to eight replicates were measured at each state point for a total of 1756 $p-\rho-T$ data. The measured points are depicted in Figure 3.

Table 2 presents data measured along pseudoisochores, and Table 3 presents measurements along isotherms. The values listed in the tables represent only one data point from the replicate measurements at a given (T, p) state. The experimental temperature and pressure are averages of the readings taken over the 12 min period needed to complete the weighings comprising a single density determination. The final column gives the relative difference between the measured densities and the equation of state of Lemmon et al.[7] All of the measured data are available as Supporting Information. Detailed comparisons with all of the available literature data are presented in the companion EOS paper;[7] summary comparisons are presented here.

These measurements will be discussed in three distinct regions. The measurements in the compressed liquid region ($\rho > 353$ kg·m^{-3} or $\rho/\rho_{crit} > 1.6$) are compared to the equation of state in Figure 4. (Note that these figures plot all of the replicate data points.) These show excellent internal consistency and agreement with the EOS. The relative standard deviation for these 416 points is 0.0018 %, and virtually all the points are within 0.0050 % of the equation of state. Given that these data

Table 2. Experimental $p-\rho-T$ Data for Propane and Relative Deviations of the Experimental Data from Densities ρ_{EOS} Calculated with the Equation of State of Lemmon et al.[7a]

T / K	p / MPa	ρ / kg·m^{-3}	$100[(\rho_{sat} - \rho_{sat,EOS})/\rho_{sat,EOS}]$	T / K	p / MPa	ρ / kg·m^{-3}	$100[(\rho_{sat} - \rho_{sat,EOS})/\rho_{sat,EOS}]$
			first filling				
319.998	10.3474	487.109	0.0022	420.004	20.9309	389.393	0.0044
339.998	19.7839	485.644	0.0028	350.004	2.8452	70.633	0.0350
349.997	24.4560	484.992	0.0028	355.005	3.0033	73.459	−0.0359
349.996	12.0702	449.429	0.0037	360.005	3.1083	73.436	−0.0158
359.996	15.7612	448.822	0.0044	369.830	3.3094	73.366	0.0001
369.822	19.3751	448.260	0.0045	380.004	3.5135	73.336	0.0042
379.997	23.0986	447.703	0.0041	400.004	3.9018	73.217	0.0160
350.001	3.5062	392.664	0.0026	420.006	4.2440	72.251	0.0168
360.003	5.9494	392.139	0.0031	440.006	4.6131	72.240	0.0079
369.828	8.3824	391.643	0.0029	460.006	4.9788	72.265	0.0017
380.003	10.9194	391.154	0.0052	480.006	5.3405	72.283	−0.0070
400.004	15.9263	390.230	0.0040	500.007	5.6977	72.281	−0.0093
			second filling				
359.002	3.4364	96.262	0.0761	420.002	1.6390	22.775	0.0253
360.001	3.4680	96.380	0.1068	440.000	1.7332	22.750	0.0193
365.003	3.6756	100.803	−0.0274	460.002	1.8307	22.779	0.0141
369.852	3.8276	100.816	−0.0131	480.003	1.9250	22.771	0.0159
375.002	3.9802	100.464	0.0045	500.001	2.0168	22.738	0.0162
380.000	4.1320	100.514	−0.0003	310.004	0.7603	14.742	−0.0166
400.003	4.6920	99.426	0.0155	315.004	0.7750	14.717	−0.0151
420.003	5.2537	99.377	0.0175	320.003	0.7894	14.690	−0.0153
440.003	5.8039	99.332	0.0163	325.004	0.8037	14.663	−0.0119
460.004	6.3456	99.291	0.0140	330.003	0.8179	14.635	−0.0113
480.006	6.8809	99.261	0.0106	340.002	0.8461	14.584	−0.0099
500.004	7.4088	99.200	0.0079	360.005	0.9012	14.483	−0.0075
340.000	2.3554	55.483	0.0982	369.854	0.9278	14.433	−0.0077
345.000	2.4949	58.079	0.0008	380.004	0.9548	14.381	−0.0085
350.003	2.5736	58.039	−0.0066	400.002	0.9590	13.553	−0.0041
355.003	2.6507	57.995	−0.0051	420.002	0.9921	13.244	−0.0017
360.003	2.7255	57.916	0.0033	440.005	1.0325	13.071	0.0002
369.850	2.8718	57.825	0.0198	460.005	1.0464	12.585	−0.0068
380.001	3.0210	57.773	0.0204	480.006	1.0393	11.906	0.0126
400.001	3.3086	57.688	0.0229	500.006	1.0587	11.589	0.0017
420.002	3.5920	57.654	0.0155	310.004	0.4606	8.455	−0.0232
440.000	3.8655	57.527	0.0042	320.003	0.4767	8.434	−0.0195
460.002	4.1235	57.223	0.0002	330.003	0.4926	8.413	−0.0169
480.002	4.3771	56.949	−0.0030	340.003	0.5083	8.392	−0.0146
500.003	4.6444	56.938	−0.0090	360.004	0.5393	8.350	−0.0138
330.002	1.7145	36.573	0.0837	369.854	0.5545	8.330	−0.0141
335.001	1.7653	36.733	0.0735	380.003	0.5699	8.309	−0.0175
340.000	1.8171	36.924	0.0686	400.004	0.6000	8.268	−0.0185
350.001	1.9425	37.864	0.0440	420.006	0.6297	8.229	−0.0170
360.002	2.0334	37.871	0.0553	440.006	0.6590	8.189	−0.0206
369.852	2.1204	37.840	0.0557	460.006	0.6877	8.149	−0.0133
380.001	2.2086	37.804	0.0508	480.004	0.7161	8.108	−0.0220
400.002	2.3803	37.749	0.0443	500.006	0.7443	8.069	−0.0235
420.001	2.5498	37.700	0.0127	310.003	0.2617	4.650	−0.0418
440.002	2.7218	37.737	−0.0007	320.004	0.2702	4.640	−0.0378
460.003	2.8925	37.772	−0.0078	330.004	0.2787	4.629	−0.0399
480.004	3.0692	37.904	−0.0098	340.003	0.2871	4.619	−0.0383
500.003	3.2435	38.005	−0.0043	360.000	0.3037	4.597	−0.0338
315.002	1.3065	27.924	0.1017	369.852	0.3119	4.587	−0.0324
320.001	1.3339	27.776	0.1500	380.002	0.3202	4.576	−0.0404
325.002	1.3406	27.079	0.1103	400.003	0.3364	4.555	−0.0398
330.002	1.3472	26.440	0.0431	420.002	0.3525	4.535	−0.0367
340.001	1.3524	25.161	0.0454	440.002	0.3683	4.514	−0.0395
360.001	1.3613	23.079	0.0408	460.005	0.3841	4.494	−0.0367
369.851	1.3874	22.639	0.0447	480.006	0.3997	4.475	−0.0373
380.001	1.4420	22.727	0.0407	500.005	0.4150	4.454	−0.0555
400.001	1.5422	22.774	0.0333				

[a] Data are along pseudoisochores, and only one point per temperature−pressure (T, p) state point is given; see Supporting Information for all data.

were one of the primary data sets for fitting the EOS in the compressed-liquid region, this excellent agreement demonstrates the repeatability of the densimeter, but it does not, however, prove that the data are correct. The density data of Glos et al.[3] and Claus et al.[4] are also compared to the EOS in Figure 4; the agreement among all three data sets is seen to be excellent. Such agreement among three data sets measured on three separate instruments (Glos et al. used a two-sinker densimeter and Claus et al. used a single-sinker densimeter) by two different laboratories using different samples does give high confidence that the experimental data and equation of state are correct. Furthermore, the equation of state was fitted to multiple properties (including density, vapor pressure, speed of sound, and heat capacity), and all the properties were fit within experimental uncertainties. Such a result is possible only if all the data are thermodynamically consistent.

Vapor-phase measurements ($\rho < 132$ kg·m^{-3} or $\rho/\rho_{crit} < 0.6$) are compared to the EOS in Figure 5. The relative deviations for these 538 points are mostly less than 0.050 %, but a significant number of points have larger relative

Table 3. Experimental $p-\rho-T$ Data for Propane and Relative Deviations of the Experimental Data from Densities ρ_{EOS} Calculated with the Equation of State of Lemmon et al.[7a]

	T	p	ρ	
	K	MPa	kg·m^{-3}	$100[(\rho_{sat} - \rho_{sat,EOS})/\rho_{sat,EOS}]$
third filling				
	265.000	3.7663	545.182	0.0023
	265.002	34.9156	582.091	0.0019
	265.000	30.0072	577.457	0.0020
	265.001	24.0302	571.371	0.0023
	265.002	20.1892	567.157	0.0027
	265.000	16.2432	562.535	0.0029
	265.002	12.1370	557.343	0.0029
	265.002	8.3319	552.121	0.0035
	265.002	4.1450	545.794	0.0037
	265.002	2.1440	542.507	0.0036
	280.003	35.4936	569.255	0.0004
	280.002	29.9022	563.397	0.0006
	280.002	24.1754	556.845	0.0010
	280.003	20.1713	551.857	0.0013
	280.002	16.0521	546.301	0.0014
	280.002	12.1656	540.568	0.0009
	280.003	8.0389	533.835	0.0020
	280.004	4.0785	526.539	0.0019
	280.003	2.0163	522.324	0.0019
	300.003	35.1525	550.916	−0.0005
	300.003	29.8918	544.528	−0.0008
	300.002	23.9089	536.476	−0.0002
	300.003	20.3696	531.214	0.0000
	300.003	16.0348	524.125	0.0000
	300.002	12.0245	516.758	−0.0001
	300.002	8.0380	508.393	0.0002
	300.002	4.0374	498.494	0.0001
	300.002	2.0967	492.918	0.0011
	320.000	35.3000	532.945	−0.0011
	320.001	29.9825	525.494	−0.0007
	320.001	24.0716	516.146	−0.0008
	320.002	20.0628	508.969	−0.0004
	320.003	16.0947	500.967	−0.0003
	320.001	12.0034	491.440	−0.0008
	320.002	8.2584	481.067	−0.0006
	320.002	4.0810	466.419	−0.0001
	320.003	2.0198	457.107	0.0009
	340.001	34.9614	514.106	−0.0010
	340.002	29.8157	505.712	−0.0008
	340.001	23.9806	494.781	−0.0001
	340.002	19.9455	486.006	0.0004
	340.000	16.0694	476.247	−0.0001
	340.002	12.0405	464.071	0.0001
	340.003	8.0538	448.649	−0.0001
	340.002	3.9256	425.072	−0.0022
	360.003	35.2601	496.073	−0.0003
	360.004	30.1267	486.462	0.0001
	360.002	23.8906	472.674	0.0007
	360.003	19.9100	462.102	0.0014
	360.002	16.0747	449.912	0.0012
	360.003	11.9232	433.101	0.0005
	360.003	7.9312	409.824	−0.0016
	380.002	34.3438	475.596	−0.0001
	380.003	29.6452	465.241	0.0006
	380.003	23.6969	449.488	0.0012
	380.004	19.8208	436.808	0.0015
	380.003	15.9450	420.987	0.0010
	380.003	11.8802	398.187	−0.0001
	380.003	7.9755	360.582	−0.0010
	400.003	35.8520	460.105	0.0002
	400.002	29.9270	445.504	0.0004
	400.004	17.4499	398.978	0.0007
	400.002	11.7907	357.333	0.0007
	400.003	7.9134	286.864	−0.0142

[a] Data are along isotherms, and only one point per temperature−pressure (T, p) state point is given; see Supporting Information for all data.

deviations, up to 0.16 %. The likely cause for the larger deviations is suggested by Figure 5c, which plots the

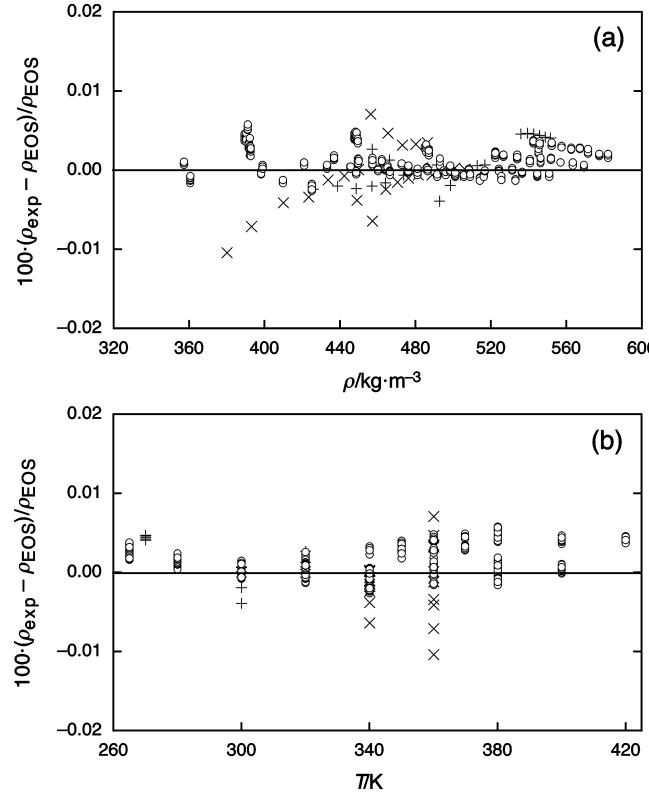

Figure 4. Relative deviations of the experimental densities ρ_{exp} for propane from values calculated with the equation of state ρ_{EOS} of Lemmon et al.[7] for liquid-phase states (ρ_{exp} > 353 kg·m^{-3}): (a) plotted as a function of density ρ and (b) plotted as a function of temperature T. ○, This work; +, Glos et al.;[3] ×, Claus et al.[4]

deviations versus pressure. All of the large deviations occur at pressures between (1.30 and 3.5) MPa, suggesting a problem with the hydrostatic head correction for the pressure, as discussed in Section 3. But even with the increased uncertainty associated with the hydrostatic head correction, the relative standard deviation of all of the vapor-phase measurements compared to the EOS is 0.035 %. For the 68 measurements at p > 4.25 MPa, the relative standard deviation is 0.010 % with a mean systematic error of +0.0031 %. For the 205 measurements at p < 1.30 MPa, the standard deviation is 0.015 % with a mean systematic error of −0.020 %. The deviations trend steadily downward with decreasing density, reaching −0.035 % to −0.056 % for the lowest-density isochore at 4.5 kg·m^{-3}.

4.3. Correction for Density Gradients and $p-\rho-T$ Data in the Extended Critical Region. The analysis presented by McLinden et al.[12] and summarized above as eqs 2 to 6 assumes that the fluid density is the same for all the weighings needed for a single density determination, and in particular, both sinkers sense the same density. The two sinkers are located one above the other in the measuring cell; the center of mass of the tantalum sinker is 4.2 cm above that of the titanium sinker. Thus, the fluid density at the tantalum sinker will be lower than that at the titanium sinker

$$\rho_{Ta} = \rho_{Ti} - \int_{h_{Ti}}^{h_{Ta}} \frac{\partial \rho}{\partial p} \rho g \cdot \mathrm{d}h \qquad (11)$$

where g is the local acceleration of gravity, $(\partial\rho/\partial p)$ is the compressibility of the fluid, and the integration is carried out between the bottom of the Ti sinker and the top of the Ta sinker.

In most cases, the correction given by eq 11 is small. For example, for low-pressure gas states approaching the ideal-gas limit

$$\frac{\partial p}{\partial \rho} = \frac{M}{RT} \tag{12}$$

where M is the molar mass, and the difference in density sensed by the two sinkers ranges from $4.4 \cdot 10^{-6} \cdot \rho$ at 500 K to $8.2 \cdot 10^{-6} \cdot \rho$ at 265 K for propane in the present instrument. For compressed-liquid states, the relative difference is less than $1 \cdot 10^{-6}$.

Near the critical point, however, the compressibility becomes large, and this effect can become significant. An indication of this effect is provided by the values of the coupling factor ϕ calculated with eq 5. Figure 6 plots ϕ as a function of density for all of the measured points. In general, ϕ is a nearly linear function of density, but near the critical density of 220.48 $kg \cdot m^{-3}$, the apparent value of ϕ increases greatly. The magnetic properties of a fluid are not affected by critical phenomena, and the large (apparent) change in ϕ is due to the different fluid densities experienced by the two sinkers, violating the assumption of constant density implicit in the analysis leading to eqs 2 to 6. This conclusion is reinforced by Figure 7, which plots ϕ as a function of the fluid compressibility—all of the anomalously large values of ϕ correspond to large values of compressibility.

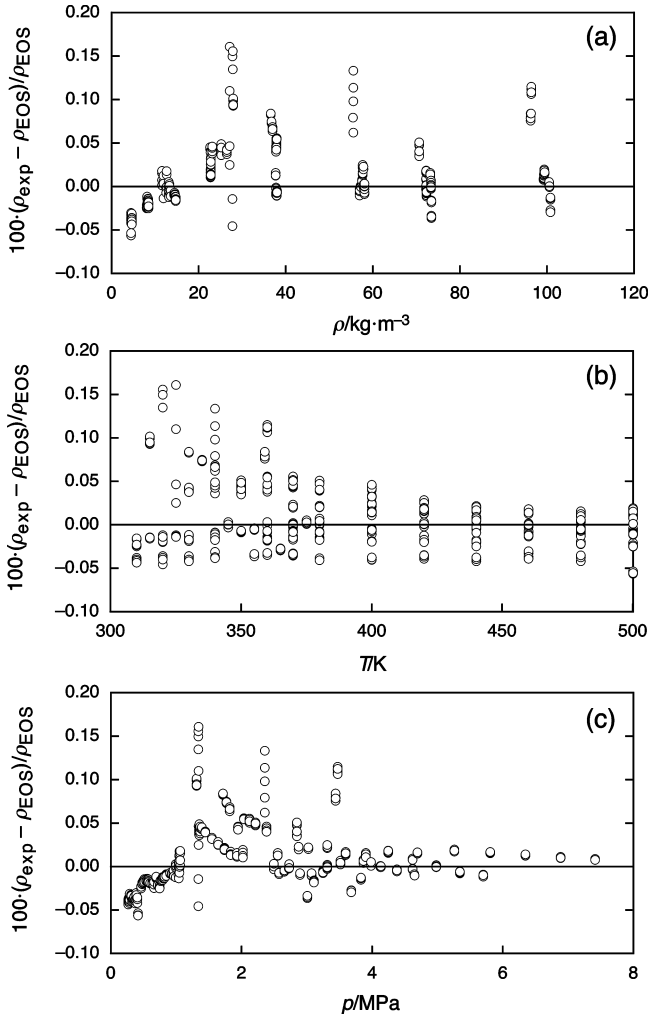

Figure 5. Relative deviations of the experimental densities ρ_{exp} for propane from values calculated with the equation of state ρ_{EOS} of Lemmon et al.[7] for vapor-phase states ($\rho_{exp} < 132$ $kg \cdot m^{-3}$): (a) plotted as a function of density ρ; (b) plotted as a function of temperature T; and (c) plotted as a function of pressure p.

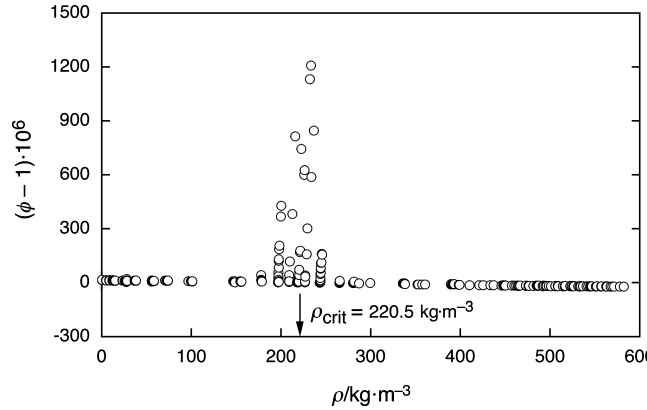

Figure 6. Values of the coupling factor ϕ for the present results for propane plotted as a function of density ρ. The critical density ρ_{crit} of 220.48 $kg \cdot m^{-3}$ is indicated.

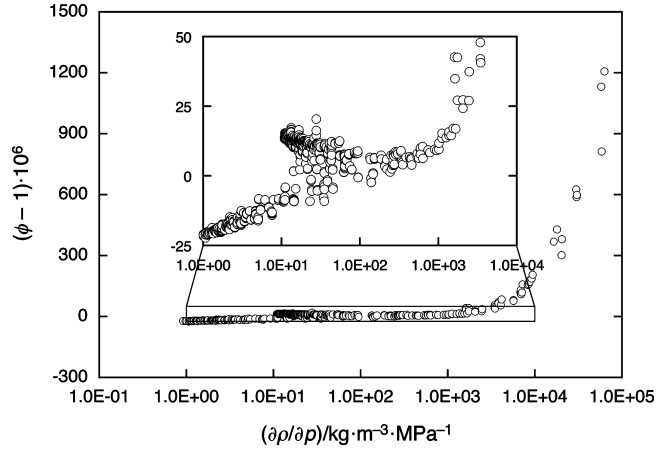

Figure 7. Values of the coupling factor ϕ for the present results for propane plotted as a function of the fluid compressibility $(\partial\rho/\partial p)$. The large values of ϕ at large $(\partial\rho/\partial p)$ are an artifact as discussed in the text. The inset provides an expanded view of the majority of the data points (i.e., those away from the critical point).

In the present work, the integral of eq 11 is approximated as

$$\rho_{Ta} \cong \rho_{Ti} - \frac{\partial \rho}{\partial p} \rho g (h_{Ta} - h_{Ti}) \tag{13}$$

where h_{Ta} and h_{Ti} are the heights of the center of mass of each sinker and the compressibility is calculated from the equation of state of Lemmon et al.[7] An initial guess for density (with $\rho_{Ta} = \rho_{Ti}$) is made using eqs 2 to 6; eq 13 is then used to refine the density values for ρ_{Ta}. The value of ϕ is obtained by fitting ϕ outside the critical region as a linear function of density. An iterative solution is required since the compressibility is a function of (T, ρ) and the density is a function of eq 13. The densities reported in this work are for ρ_{Ti} at the pressure corresponding to the height of the titanium sinker in the measuring cell. In the absence of this correction, the densities would have been in error by the factor $(\phi - 1)$ or as much as $0.0012 \cdot \rho$, very near the critical point.

Measurements in the extended critical region ($132 < \rho/kg \cdot m^{-3} < 353$ or $0.60 < \rho/\rho_{crit} < 1.6$) are listed in Table 4 and compared to the EOS in Figure 8. For these points, comparisons are made in terms of deviations in the measured pressure compared with the pressures calculated with the EOS as a function of T and ρ. Because of the "flatness" of the isotherms near the critical point, comparisons of densities as a $f(T, p)$ are less meaningful in this region. The standard deviation in pressure for the 527 measured points is $110 \cdot 10^{-6} \cdot p$, with a systematic error of $-78 \cdot 10^{-6} \cdot \rho$.

This instrument was not designed to study critical phenomena. The near-critical measurements carried out in this work were intended to investigate how close to the critical point meaningful density measurements could be made. As discussed in the companion EOS paper,[7] the uncertainties increase substantially as the critical point is approached. Nevertheless, the present data were used, together with the EOS model, to determine the critical parameters of propane as detailed by Lemmon et al.[7]

$T_{crit} = (369.89 \pm 0.03)$ K;
$\rho_{crit} = (5.00 \pm 0.04)$ mol·L^{-1} [$= (220.48 \pm 1.76)$ kg·m^{-3}];
$p_{crit} = (4.2512 \pm 0.0050)$ MPa

The expanded ($k = 2$) uncertainties in these values are comparable to those of many direct measurements of the critical point.

Table 4. Experimental $p-\rho-T$ Data for Propane in the Near-Critical Region ($132 < \rho/\text{kg·m}^{-3} < 353$) and Relative Deviations of the Experimental Data from Pressures p_{EOS} Calculated with the Equation of State of Lemmon et al.[7a]

T/K	p/MPa	ρ/kg·m^{-3}	$100[(\rho_{sat} - \rho_{sat,EOS})/\rho_{sat,EOS}]$	T/K	p/MPa	ρ/kg·m^{-3}	$100[(\rho_{sat} - \rho_{sat,EOS})/\rho_{sat,EOS}]$
			first filling				
365.003	4.2013	337.537	−0.0308	400.004	6.6304	219.388	−0.0226
369.828	4.9860	337.358	−0.0284	420.004	8.2285	219.042	−0.0342
375.003	5.8439	337.161	−0.0250	440.003	9.8267	218.701	−0.0362
380.003	6.6843	336.970	−0.0215	460.004	11.4199	218.352	−0.0309
400.006	10.1121	336.235	−0.0255	480.005	13.0073	218.014	−0.0111
420.006	13.5930	335.538	−0.0198	500.004	14.5822	217.645	0.0012
369.004	4.1980	281.207	0.0056	369.827	4.2456	199.849	−0.0134
369.830	4.2847	281.220	−0.0028	369.927	4.2528	197.901	−0.0081
372.004	4.5177	281.200	−0.0086	370.027	4.2600	197.162	−0.0057
375.004	4.8469	281.140	−0.0116	370.327	4.2813	196.772	−0.0011
380.002	5.4083	280.989	−0.0148	370.824	4.3167	196.709	0.0048
400.001	7.7369	280.447	−0.0228	371.827	4.3874	196.803	0.0058
420.003	10.1265	279.935	−0.0327	375.001	4.6097	197.026	0.0011
369.828	4.2469	245.368	0.0003	380.002	4.9578	197.115	−0.0023
369.928	4.2551	244.551	−0.0037	400.002	6.3384	196.877	−0.0195
370.028	4.2634	244.214	−0.0065	420.004	7.7097	196.605	−0.0291
370.328	4.2886	243.827	−0.0126	369.002	4.1437	146.444	−0.0019
370.828	4.3310	243.648	−0.0173	369.827	4.1862	146.570	−0.0065
371.827	4.4167	243.586	−0.0212	370.329	4.2122	146.684	−0.0059
375.001	4.6945	243.594	−0.0182	370.828	4.2383	146.892	−0.0072
380.003	5.1416	243.563	−0.0138	371.826	4.2936	147.930	0.0025
400.002	6.9786	243.192	−0.0205	375.002	4.4550	148.082	0.0025
420.004	8.8480	242.768	−0.0353	380.002	4.7038	148.075	0.0007
369.928	4.2540	232.121	−0.0069	400.003	5.6685	147.916	−0.0055
370.028	4.2617	225.730	−0.0091	420.006	6.6060	147.759	−0.0089
370.327	4.2848	221.028	−0.0085	440.005	7.5268	147.611	−0.0124
370.828	4.3234	219.823	−0.0091	460.008	8.4351	147.462	−0.0144
371.827	4.4009	219.642	−0.0094	480.005	9.3308	147.278	−0.0150
375.003	4.6487	219.656	−0.0084	500.005	10.2185	147.114	−0.0130
380.004	5.0417	219.678	−0.0108				
			second filling				
360.003	3.7309	352.636	−0.0139	370.851	4.3228	208.990	0.0049
369.855	5.5206	352.210	−0.0107	371.853	4.3972	208.907	0.0049
369.852	5.0125	338.099	−0.0061	375.004	4.6311	208.972	0.0017
369.854	4.3732	299.082	0.0040	380.002	5.0022	208.942	0.0005
369.855	4.2588	265.229	0.0087	369.851	4.2418	177.526	−0.0004
369.956	4.2682	265.215	0.0047	369.951	4.2484	177.657	0.0007
370.054	4.2775	265.206	0.0046	370.050	4.2549	177.695	0.0036
370.352	4.3059	265.204	0.0030	370.352	4.2744	177.808	0.0063
370.853	4.3538	265.195	−0.0016	370.851	4.3066	177.874	0.0110
371.853	4.4504	265.134	−0.0045	371.852	4.3705	178.012	0.0118
375.002	4.7617	265.094	−0.0021	375.001	4.5690	178.185	0.0087
380.003	5.2686	264.991	−0.0002	379.999	4.8795	178.216	0.0044
369.855	4.2487	234.526	0.0051	369.852	4.1883	146.912	−0.0129
369.954	4.2564	231.817	−0.0001	370.350	4.2143	147.029	−0.0113
370.054	4.2643	229.062	0.0002	370.850	4.2408	147.314	−0.0119
370.354	4.2879	227.342	−0.0043	371.849	4.2958	148.252	−0.0035
370.856	4.3276	226.673	−0.0066	374.999	4.4561	148.366	−0.0022
371.853	4.4072	226.521	−0.0055	380.001	4.7056	148.360	−0.0045
375.004	4.6609	226.503	−0.0047	400.003	5.6732	148.236	−0.0105
380.002	5.0679	226.420	−0.0028	420.001	6.6131	148.070	−0.0111
369.852	4.2482	220.705	−0.0004	440.003	7.5360	147.904	−0.0151
369.953	4.2558	214.471	−0.0028	460.001	8.4450	147.718	−0.0169
370.053	4.2633	211.466	−0.0007	480.002	9.3439	147.549	−0.0168
370.353	4.2857	209.496	0.0013	500.003	10.2340	147.392	−0.0167
			fourth filling				
380.002	4.7557	155.492	0.0030	459.999	8.7319	154.768	−0.0137
400.002	5.7816	155.313	−0.0065	479.998	9.6901	154.579	−0.0121
420.001	6.7805	155.129	−0.0085	499.999	10.6373	154.378	−0.0147
440.002	7.7626	154.945	−0.0123	399.998	5.6772	148.477	−0.0036

[a] Data are along pseudoisochores, and only one point per temperature−pressure (T, p) state point is given; see Supporting Information for all data.

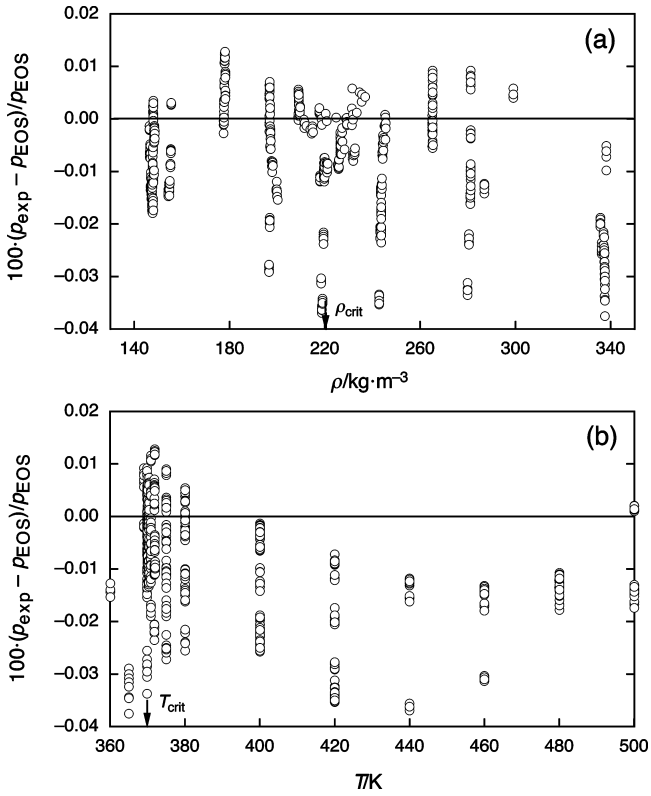

Figure 8. Relative deviations of the experimental pressures p_{exp} for propane from values calculated with the equation of state p_{EOS} of Lemmon et al.[7] taking the measured temperature and density as the independent variables for states in the extended critical region ($132 < \rho_{exp}/kg\cdot m^{-3} < 353$): (a) plotted as a function of density ρ and (b) plotted as a function of temperature T.

4.4. Comparison of Measurement Uncertainties to EOS Fit. A very useful and informative way of evaluating the fit of the data to the equation of state is to examine the ratio of the deviations of the data points from the equation of state with the combined standard ($k = 1$) uncertainty given by eq 8 or 9

$$t = \frac{\rho_{exp} - \rho_{EOS}}{u_C(\rho)} \quad \text{or} \quad t = \frac{p_{exp} - p_{EOS}}{u_C(p)} \qquad (14)$$

This ratio is plotted in Figure 9. For 1705 out of the total of 1756 data points (97.1 %), this ratio is less than ± 2.0, and this is typically interpreted as "fitting the equation of state within the uncertainty of the data". Virtually all of the points with $t > 2$ or $t < -2$ lie within the pressure range $1.30 < p/MPa < 3.5$ for the reasons discussed in Section 4.2. All of the liquid-phase data fall well within the estimated uncertainty. The comparatively large relative deviations for the very low density isochores are seen to be within the experimental uncertainties. Likewise, all of the near-critical points are well fit. This comparison lends credence to the estimated uncertainties of both the experimental data and the equation of state.

5. Discussion and Conclusions

High accuracy $p-\rho-T$ data were measured for propane. These complemented literature data and filled in gaps in the extended critical region, enabling the development of an equation of state that is among the most accurate currently available for any fluid. Vapor pressures were also measured, although uncertanties in the hydrostatic head correction make the present apparatus less than optimal for vapor pressures less than about 1 MPa.

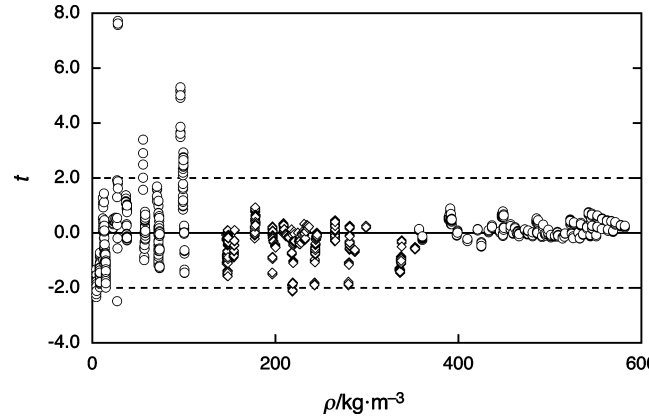

Figure 9. Ratio t of the deviation of the measured points from the equation of state of Lemmon et al.[7] to the experimental uncertainty as a function of density ρ. ○, Deviations in density taking the measured temperature and pressure as the independent variables ($t = (\rho_{exp} - \rho_{EOS})/u_C(\rho)$); ◇, deviations in pressure taking the measured temperature and density as the independent variables ($t = (p_{exp} - p_{EOS})/u_C(p)$). The dashed lines indicate ± 2 times the standard uncertanties.

Densities as low as 4.45 $kg\cdot m^{-3}$ were measured. Data at such low densities are of limited utility in fitting an equation of state—the fluid must approach the ideal-gas limit. These measurements were done, in part, to explore the low-density capabilities of the densimeter. Likewise, although the two-sinker densimeter used here was not intended for critical-region studies, it was successfully applied in the vicinity of the critical point—measurements along the critical isochore started at T_{crit} + 0.035 K, and measurements at the critical temperature were made at $0.95\cdot\rho_{crit}$ and $1.05\cdot\rho_{crit}$. The data were used, in conjunction with the fitting of the EOS, to determine the critical parameters. The advantage of determining critical-point parameters in this way is that they are entirely consistent with the $p-\rho-T$ data on which the EOS is based.

Uncertainties associated with the hydrostatic head correction for pressure led to increased errors in the $p-\rho-T$ data in the vapor phase for $1.30 < p/MPa < 4.25$ and for vapor pressures at temperatures less than about 340 K. Ideally, the pressure transducer and all connecting lines would be located at the same height as the measuring cell. An alternative would be to use a differential pressure cell with a noncondensing gas transmitting the pressure to the transducer. Various design constraints prevented doing this, but after measuring propane, the filling line was reconfigured so that more of the temperature gradient between the measuring cell and pressure transducer occurs in a horizontal section. The increased uncertainties apply only for fluids that condense (or vaporize) along the length of the filling line, and the modification to the filling line should reduce these uncertainties for such fluids measured in the future.

In this work, the measurements and equation of state development occurred simultaneously, and this had significant benefits. The extensive literature survey and data evaluation that were part of the EOS development identified the (T, p) regions where new data were most needed. As the EOS fitting proceeded, there were several instances where additional measurements were added to the original test plan to resolve conflicts between different literature data sets or to provide data in regions where the EOS had significant curvature. The availability of preliminary EOS fits aided in the analysis of the experimental data.

Supporting Information Available:

The data tabulations in this paper report only a single measurement at each (T, p) state point. Four or more replicate measurements

were made at each state point, and all of the data are included. More details on uncertainties are provided, including the temperature, pressure, density, and combined uncertainties for each measured point. The standard deviation in the measured quantities (that is, a measure of the scatter in the multiple temperature and pressure readings carried out for each density determination) is also reported. This material is available free of charge via the Internet at http://pubs.acs.org.

Literature Cited

(1) Bücker, D.; Wagner, W. A reference equation of state for the thermodynamic properties of ethane for temperatures from the melting line to 675 K and pressures up to 900 MPa. *J. Phys. Chem. Ref. Data* **2006**, *35*, 205.

(2) Bücker, D.; Wagner, W. Reference equations of state for the thermodynamic properties of fluid phase n-butane and isobutane. *J. Phys. Chem. Ref. Data* **2006**, *35*, 929.

(3) Glos, S.; Kleinrahm, R.; Wagner, W. Measurement of the (*p, ρ, T*) relation of propane, propylene, n-butane, and isobutane in the temperature range from (95 to 340) K at pressures up to 12 MPa using an accurate two-sinker densimeter. *J. Chem. Thermodyn.* **2004**, *36*, 1037–1059.

(4) Claus, P., Schilling, G., Kleinrahm, R. and Wagner, W. Internal Report. Ruhr-Universität Bochum, 2002. (These data are also reported by Glos et al.[3])

(5) Meier, K. Thermodynamic properties of propane. IV. Speed of sound measurements. *J. Chem. Eng. Data*, submitted for publication.

(6) Perkins, R. A.; Sanchez Ochoa, J. C.; Magee, J. W. Thermodynamic properties of propane. II. Specific heat capacity at constant volume from (85 to 345) K with pressures to 35 MPa. *J. Chem. Eng. Data*, **2009**, accepted.

(7) Lemmon, E. W.; McLinden, M. O.; Wagner, W. Thermodynamic properties of propane. III. Equation of state. *J. Chem. Eng. Data* **2009**, accepted.

(8) Kleinrahm, R.; Wagner, W. Measurement and correlation of the equilibrium liquid and vapour densities and the vapour pressure along the coexistence curve of methane. *J. Chem. Thermodyn.* **1986**, *18*, 739–760.

(9) Wagner, W.; Kleinrahm, R. Densimeters for very accurate density measurements of fluids over large ranges of temperature, pressure, and density. *Metrologia* **2004**, *41*, S24–S39.

(10) McLinden, M. O.; Lösch-Will, C. Apparatus for wide-ranging, high-accuracy fluid (*p-ρ-T*) measurements based on a compact two-sinker densimeter. *J. Chem. Thermodyn.* **2007**, *39*, 507–530.

(11) Lösch-Will, C. Ph.D. thesis, Lehrstuhl für Thermodynamik, Ruhr-Universität Bochum, Germany, 2005.

(12) McLinden, M. O.; Kleinrahm, R.; Wagner, W. Force transmission errors in magnetic suspension densimeters. *Int. J. Thermophys.* **2007**, *28*, 429–448.

(13) Bruno, T. J.; Svoronos, P. D. N. *CRC Handbook of Basic Tables for Chemical Analysis*, 2nd ed.; Taylor and Francis CRC press: Boca Raton, FL, 2004.

(14) Bruno, T. J.; Svoronos, P. D. N. *CRC Handbook of Fundamental Spectroscopic Correlation Charts*; Taylor and Francis CRC press: Boca Raton, FL, 2005.

(15) McLinden, M. O.; Splett, J. D. A liquid density standard over wide ranges of temperature and pressure based on toluene. *J. Res. NIST* **2008**, *113*, 29–67.

(16) Bowman, H. A.; Schoonover, R. M.; Carroll, C. L. A density scale based on solid objects. *J. Res. NBS* **1973**, *78A*, 13–40.

(17) Bowman, H. A.; Schoonover, R. M.; Carroll, C. L. The utilization of solid objects as reference standards in density measurements. *Metrologia* **1974**, *10*, 117–121.

(18) McLinden, M. O. Densimetry for primary temperature metrology and a method for the *in-situ* determination of densimeter sinker volumes. *Meas. Sci. Technol.* **2006**, *17*, 2597–2612.

Received for review January 29, 2009. Accepted May 6, 2009. This work was supported, in part, by the United States Department of Energy.

JE900124N